Int. J. Heat Mass Transfer. Vol. 34, No. 4/5, pp. 1043–1057, 1991
Printed in Great Britain

0017–9310/91 $3.00 + 0.00

Heat transfer in membrane waterwalls

B. D. BOWEN,† M. FOURNIER‡ and J. R. GRACE†
† Department of Chemical Engineering, The University of British Columbia, Vancouver, Canada V6T 1W5
‡ Domtar Research Centre, Senneville, Canada H9X 3L7

(*Received* 7 *February* 1990 *and in final form* 5 *June* 1990)

Abstract—Conduction heat transfer in membrane waterwall assemblies consisting of tubes connected by longitudinal fins is analysed for conditions typical of fluidized bed boilers. Four approximate analytic models are derived together with an exact numerical model which employs a finite difference method and a boundary-fitted orthogonal coordinate transformation. The approximate models generally improved in accuracy as their degree of sophistication increased. A range of conditions is considered to demonstrate the influence of such factors as tube thickness, fin thickness and width, inside and outside heat transfer coefficients and tube and wall thermal conductivities on the overall heat transfer coefficient. The effectiveness of the fin and of the insulated sector of the tube are shown to be closely related.

INTRODUCTION

MEMBRANE waterwalls, consisting of parallel tubes connected longitudinally by fins or membrane bars, have long been a feature of many pulverized coal combustion boilers and of recovery boilers used in the pulp and paper industry [1, 2]. Insulated on one side and exposed to the furnace on the other, these walls provide an effective means of transferring heat from a furnace operating at typical temperatures of 1750–1850 K to water being boiled or simply heated on the inside of the tubes. The walls are also used to contain the furnace, and boiler-makers have devised techniques not only for fabricating vertical membrane walls (with the tubes usually oriented vertically), but also for forming horizontal and sloping sections.

Membrane waterwalls are also commonly used to contain and extract heat from large-scale fluidized bed combustors (FBCs), operated as conventional bubbling beds (e.g. ref. [3]) or as circulating beds (e.g. ref. [4]). For large FBC installations, membrane walls may also be hung from above or supported from the sides to provide additional area for heat transfer. At the high temperatures found in pulverized coal and recovery furnaces, radiation is the predominant mechanism of furnace-to-wall heat transfer. As a consequence, local furnace-side transfer coefficients are nonuniform due to the third power dependency on temperature and to view factor variations. Fluidized boilers operate at much lower temperatures, typically 1100–1150 K. For bubbling bed units, heat transfer on the furnace side is controlled by convection, with radiation contributing no more than 15–20% to the total transfer [5]. The dense bed contacts the entire membrane surface in a relatively uniform manner, providing only that the bed covers the waterwall and that the fin width is much larger than the particle diameter. While radiation plays a larger role for circulating fluidized bed boilers, especially at low load conditions [6], recent evidence [7] suggests that local furnace-side convection coefficients will be highest in the fin region, where downward-moving strands of particles are protected by the adjacent tubes, while local radiative transfer coefficients are likely to be highest at the crests of the tubes where the solids viewed are at the core temperature. The present study considers only the limiting case where heat transfer coefficients on the furnace side can be considered to be uniform. This is believed to be a reasonable approximation for many FBC units. In future work, we intend to examine the influence of non-uniform furnace-side coefficients due to radiant interchange and/or varying bed-to-surface contacting patterns in order to make the analysis more applicable to pulverized coal furnaces, recovery boilers and circulating fluidized bed boilers operated at low or high load.

While boiler-makers undoubtedly have methods for analysing heat transfer in membrane wall assemblies, there is surprisingly little information in the open literature. Some efforts to model conduction within the wall have been reported (e.g. refs. [8, 9]) in connection with the positioning of thermocouples or other devices for measuring heat transfer rates. However, few details have been provided and there appear to be no comprehensive reports published on alternative methods for estimating heat transfer rates in such assemblies or on their reliability for design calculations. The purpose of the present paper is to at least partially redress this situation.

In the sections which follow, five different models are developed for predicting heat fluxes and overall heat transfer coefficients through membrane waterwalls with uniform inside and outside transfer coefficients. Because of the geometric complexity and discontinuous properties of the fin–tube assembly, a completely rigorous analysis of the waterwall conduction problem requires the use of numerical methods. The 'exact' numerical solution is referred to

NOMENCLATURE

$a_{11}, a_{12}, a_{21}, a_{22}$ dimensionless constants given by equations (22)
A dimensionless constant given by equation (21)
Bi tube outside Biot number, $h_o R_o/k_t$
E enhancement ratio, hemi-cylinder half-fin heat transfer rate/heat transfer rate for corresponding unfinned quarter-tube
h_i, h_o inside, outside heat transfer coefficient [W m^{-2} K^{-1}]
h_ξ, h_η dimensionless orthogonal coordinate transformation metrics
k thermal conductivity [W m^{-1} K^{-1}]
L transfer surface length parallel to tubes [m]
m dimensionless constant given by equation (13)
q dimensionless heat transfer flux, $q' R_o/k_t(T'_o - T'_i)$
q' heat transfer flux [W m^{-2}]
$\hat{q}$ dimensionless heat transfer rate, $\hat{q}'/k_t L(T'_o - T'_i)$
$\hat{q}'$ heat transfer rate [W]
r dimensionless radial coordinate, r'/R_o
r' radial coordinate (see Fig. 1) [m]
R tube radius [m]
S_1, S_2 dimensionless constants defined by equations (21)
t half-thickness of fin (see Fig. 1) [m]
T dimensionless temperature, $(T' - T'_i)/(T'_o - T'_i)$
$\bar{T}$ average dimensionless temperature at exposed tube surface or fin–tube junction
T' local temperature in fin or tube [K]
T'_i bulk temperature of coolant inside tube [K]
T'_o bulk temperature of gas–solid suspension on furnace side [K]
U_0 overall heat transfer coefficient based on projected area [W m^{-2} K^{-1}]
w half-width of fin (see Fig. 1) [m]
x, y dimensionless coordinates, x'/R_o and y'/R_o
x', y' Cartesian coordinates (see Fig. 1) [m].

Greek symbols

α dimensionless inner tube radius, R_i/R_o
β dimensionless fin half-thickness, t/R_o
γ dimensionless fin half-width, w/R_o
δ dimensionless inside heat transfer coefficient, h_i/h_o
ε dimensionless fin thermal conductivity, k_f/k_t
θ angular coordinate (see Fig. 1)
η, ξ dimensionless transformed coordinates
κ dimensionless effective heat transfer coefficient at fin–tube junction, h_f/h_o
λ_n dimensionless eigenvalues obtained by solving equation (28)
Λ_n dimensionless constants given by equation (21)
ϕ angle subtended by base of fin at tube centre (see Fig. 1)
ω value of θ at corner of fin (see Fig. 1).

Subscripts

av average value
e exposed outer surface of tube
f fin, pertaining to finned surface of tube
i inner
o outer
qt quarter-tube (unfinned)
t tube.

as Model 5 and is obtained by employing a finite difference technique in conjunction with a boundary-fitted orthogonal coordinate transformation in the fin to accommodate the curved interface adjoining the tube. Since finite difference solutions are too computationally intensive for design purposes, four analytic or semi-analytic approximations (labelled Models 1–4 in increasing order of sophistication) are also provided. Model 1 is based on the standard textbook treatment [10, 11] for finned surfaces, while Models 2–4 progressively relax some of its more restrictive assumptions. The applicability of the various approximate models is assessed by comparing their predictions with those obtained using Model 5. Finally, the Model 5 results are examined for conditions typical of fluidized bed boilers and for ranges of other conditions to determine the influence of various design factors on the heat transfer performance of membrane waterwalls.

THEORY

A cross-sectional view of a typical membrane waterwall is illustrated in Fig. 1(a). Because of symmetry considerations, only the shaded portion of the fin–tube assembly needs to be analysed in detail. Figure 1(b) is an enlarged view showing the physical dimensions and coordinates of the hemi-cylinder and half-fin which make up the shaded section. To account for the fact that heat is normally transferred from the hot combustion medium on the furnace side to the water passing through the tubes, it is assumed that the outside bulk temperature, T'_o, always exceeds the tube-side bulk temperature, T'_i.

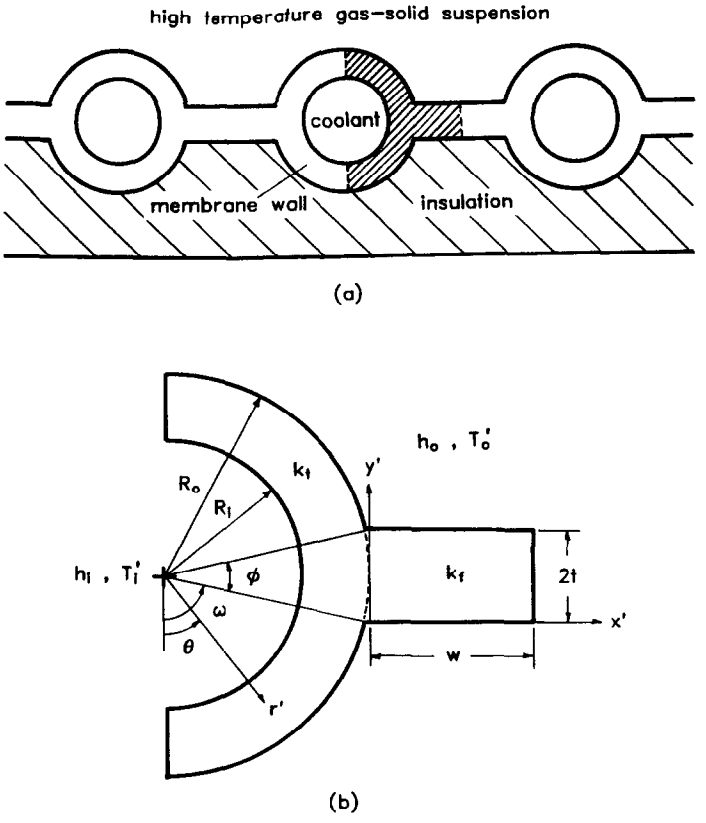

FIG. 1. Membrane wall assembly: (a) representative wall section showing portion (shaded) treated in analyses; (b) coordinate systems and dimensions.

For convenience, the membrane wall conduction problem is described in terms of the following dimensionless variables:

$$T = (T' - T_i')/(T_o' - T_i'), \quad r = r'/R_o, \quad x = x'/R_o,$$

$$y = y'/R_o, \quad \alpha = R_i/R_o, \quad \beta = t/R_o, \quad \gamma = w/R_o,$$

$$\delta = h_i/h_o, \quad \varepsilon = k_f/k_t, \quad \kappa = h_f/h_o, \quad Bi = h_o R_o/k_t,$$

$$q = q' R_o/[k_t(T_o' - T_i')], \quad \hat{q} = \hat{q}'/[k_t L(T_o' - T_i')] \qquad (1)$$

where $T'[= T_t'(r', \theta)$ or $T_f'(x', y')]$ is the dimensional local temperature (in the tube or the fin, respectively), q' and $\hat{q}'$ the dimensional heat flux and heat transfer rate, respectively, h_f a coefficient (based on the area $2tL$) which characterizes the rate of heat transfer through the fin and L the length of the membrane wall in the direction of water flow. The angle ϕ, which subtends the base of the fin, is therefore given by

$$\phi = 2 \sin^{-1}(\beta) \qquad (2)$$

while the angle ω, which determines the arc-length of both the insulated and exposed portions of the half-tube is

$$\omega = (\pi - \phi)/2. \qquad (3)$$

In addition to the specific assumptions which distinguish them, the five membrane wall heat transfer models developed below all share the following set of general assumptions:

(i) steady-state conditions prevail,

(ii) the properties of the fin and tube materials are isotropic and temperature independent,

(iii) the contact resistance at the junction of the fin and tube is insignificant,

(iv) the local coefficient for heat transfer between the tube and the water, h_i, is uniform over the inner surface,

(v) the local coefficient for heat transfer between the furnace and the exposed outer surfaces of the tube and the fin, h_o, is also uniform,

(vi) fouling on the inside of the tube and any changes on the furnace side (e.g. due to erosion, corrosion, slagging or deposition) are insignificant, and

(vii) the insulated surfaces of the tube and fin are adiabatic.

Model 1. *Tube-pure-radial, fin-one-dimensional model*

The standard textbook method [10, 11] for analysing finned surface heat transfer is to treat each separate transfer path as a one-dimensional resistor and to determine its contribution to the overall rate by means of analogies to electric circuit theory. This treatment is adopted as Model 1 and its circuit ana-

logue is illustrated in Fig. 2(a). Heat is transferred from the hot gas–solid suspension to the outer surface of the tube via two parallel paths: directly to the exposed tube surface and indirectly via the exposed surface of the fin and along the fin by conduction. Heat then flows radially inwards by conduction from the outer tube surface (at T_{to}) to its inner surface (at T_{ti}) and is finally transferred by convection to the internal coolant.

Model 1 further assumes that the fin is sufficiently thin ($\beta \ll 1$) and its Biot number sufficiently small ($Bi/\varepsilon \ll 1$) that the fin can be treated as a one-dimensional rectangular conductor. Under these conditions, the heat transfer rate through the fin, $\hat{q}'_f$, is given by

$$\hat{q}'_f = h_f \phi R_o L(T'_o - T'_{to}) = \frac{k_t L(T'_o - T'_i)(1 - T_{to})}{k_t/(\phi\kappa h_o R_o)} \quad (4)$$

or, in dimensionless terms, by

$$q'_f = \frac{(1 - \cdot}{1/(\phi\kappa\, Bi)}$$

where

$$\kappa = \left(\frac{\varepsilon}{2\beta\, Bi}\right)^{1/2} \tanh\left[\left(\frac{Bi}{2\beta\varepsilon}\right)^{1/2}\right] \quad (6)$$

for a one-dimensional rectangular fin with one exposed surface and an adiabatic tip.

Expressions similar to equation (5), involving ratios of temperature difference and thermal resistance, can be written for the other heat transfer paths which comprise the model. The thermal resistances are shown in Fig. 2(a). Using the rules of electric circuit analysis, it is straightforward to prove that the overall

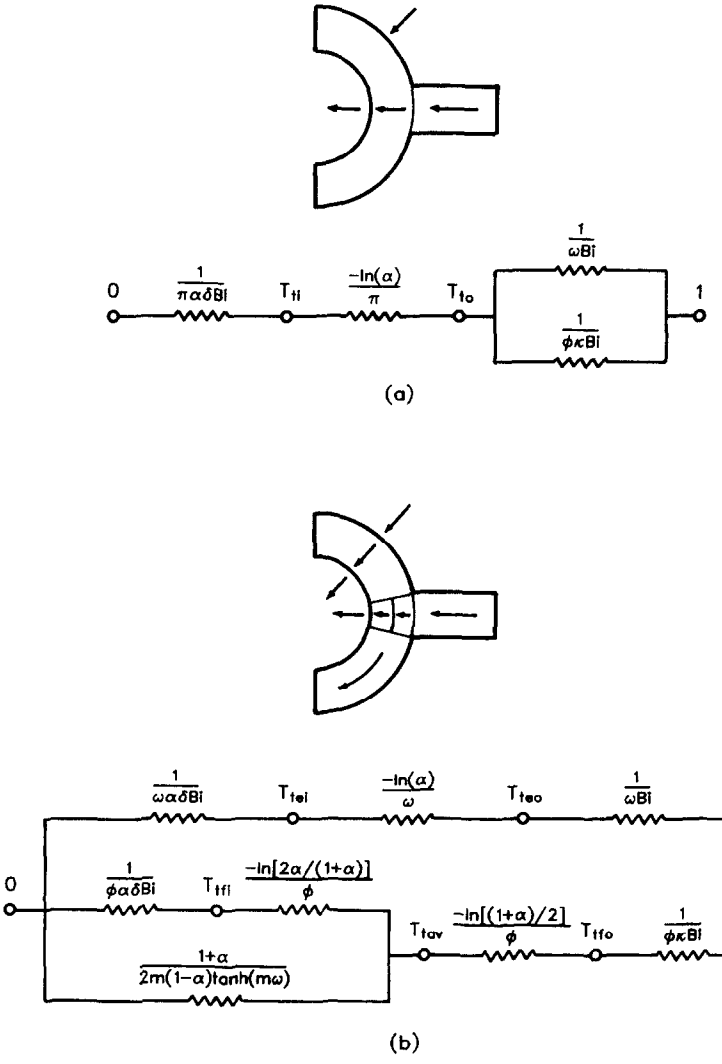

FIG. 2. Electrical circuit analogues showing dimensionless temperatures at nodes and dimensionless resistances: (a) for Model 1; (b) for Model 2.

heat transfer rate through the fin–tube assembly is given by

$$\hat{q} = \frac{1}{\dfrac{1}{\pi\alpha\delta\, Bi} - \dfrac{\ln\alpha}{\pi} + \dfrac{1}{(\omega+\kappa\phi)\, Bi}}. \tag{7}$$

Standard practice amongst boiler designers is to express the heat transfer rate in terms of an overall coefficient, U_0, based on the exposed surface area projected normal to the plane of the waterwall, i.e.

$$\hat{q} = \frac{U_0 R_o}{k_t}(1+\gamma). \tag{8}$$

When equations (7) and (8) are combined, the overall coefficient (in dimensionless form) is obtained explicitly as

$$\frac{U_0 R_o}{k_t} = \frac{\pi\, Bi/(1+\gamma)}{\dfrac{1}{\alpha\delta} - Bi\ln\alpha + \dfrac{\pi}{\omega+\kappa\phi}}. \tag{9}$$

In order to determine the effectiveness of the fin and the non-exposed portion of the tube in improving heat flow through the assembly, it is useful to define an enhancement ratio, E, as the heat transfer rate with the fin and insulated portion present to that which would occur in their absence. If neither contribution were present, the assembly heat transfer rate would be equal to that of a quarter-tube for which

$$\hat{q}_{qt} = \frac{\pi\, Bi/2}{\dfrac{1}{\alpha\delta} - Bi\ln\alpha + 1}. \tag{10}$$

Thus, the enhancement ratio for all models is given by

$$E = (1+\gamma)\frac{U_0 R_o}{k_t}\Big/\hat{q}_{qt}. \tag{11}$$

Once the overall rate is known, the separate energy flows through each path can be calculated by finding the intermediate temperatures and then applying the thermal analogue of Ohm's law.

Model 2. Exposed-tube-radial, insulated-tube-tangential, fin-one-dimensional model

Model 2 also uses an electric circuit analogue, but one which more realistically represents the membrane wall configuration. Since the outer tube surface is insulated over $0 \leqslant \theta \leqslant \omega$, conduction in this section occurs predominantly in the tangential direction. If it is assumed that only tangential conduction is admitted in this region, that radial positions in the tube section can be approximated by the average value, $(1+\alpha)/2$, and that the temperature at $\theta = \omega$ is equal to the constant value, T_{tav}, then the angular temperature distribution for $0 \leqslant \theta \leqslant \omega$ is given by

$$T_t(\theta) = T_{tav}\cosh(m\theta)/\cosh(m\omega) \tag{12}$$

where

$$m = \left[\frac{\alpha\delta\, Bi(1+\alpha)}{2(1-\alpha)}\right]^{1/2}. \tag{13}$$

The rate at which the insulated tube segment dissipates heat to the inside fluid can now be determined from the conduction rate through the radial thickness $(1-\alpha)$ at $\theta = \omega$, i.e.

$$\hat{q} = \frac{(T_{tav}-0)}{\dfrac{1+\alpha}{2(1-\alpha)m\tanh(m\omega)}} \tag{14}$$

which has the usual form of a temperature difference divided by a thermal resistance.

This angular resistance must now be combined with other thermal resistances to form the circuit analogue which best represents the whole assembly. The optimal arrangement, suggested by the numerical results described later, is illustrated in Fig. 2(b). For $\omega+\phi \leqslant \theta \leqslant \pi$, heat flows by convection from the furnace to the outside of the tube (at T_{teo}), by radial conduction to the inside surface (at T_{tei}), and then by convection from the inner surface to the coolant. Heat also passes from the gas–solid suspension through the one-dimensional fin to the fin–tube junction (at T_{tfo}) and thence, radially inwards to the centre of the tube wall (at T_{tav}). From here, it transfers to the inside fluid via two parallel paths: for $0 \leqslant \theta \leqslant \omega$, by conduction and convection through the insulated portion of the tube and for $\omega \leqslant \theta \leqslant \omega+\phi$, by radial conduction to the inside tube surface (at T_{tfi}) and then by convection. Application of the usual combinatory rules to the circuit shown in Fig. 2(b) yields the following expression for the dimensionless heat transfer coefficient:

$$\frac{U_0 R_o}{k_t} = \frac{Bi}{1+\gamma}\,\frac{\phi}{\dfrac{1}{\dfrac{\alpha\delta}{1-\alpha\delta\, Bi\ln\left(\dfrac{2\alpha}{1+\alpha}\right)} + \dfrac{2(1-\alpha)m\tanh(m\omega)}{(1+\alpha)\phi\, Bi}} - Bi\ln\left(\dfrac{1+\alpha}{2}\right) + \dfrac{1}{\kappa}} + \frac{\omega}{\dfrac{1}{\alpha\delta} - Bi\ln\alpha + 1}. \tag{15}$$

Model 3. Tube-two-dimensional, fin-one-dimensional model

Since conduction occurs tangentially in the insulated portion of the tube and radially in the exposed section, there must be a transition region in the vicinity

of the fin. In Model 3, therefore, the half-tube is treated as a two-dimensional conductor while heat transfer in the fin remains one-dimensional.

The tube conduction problem can be resolved analytically only if either the temperature or the heat flux distribution is prescribed over its entire outer surface. Because the actual heat flux is known over at least a portion of that surface, the latter condition is employed here. The following simple distribution is assumed: the heat flux is taken to be zero over the insulated section, constant at q_f over the finned section and constant at q_e over the exposed section. The latter two initially unknown fluxes can then be determined explicitly by matching the average temperatures and fluxes on either side of the finned and exposed surfaces, respectively. Sparrow and Lee [12] proposed a similar idea for analysing the heat transfer in tubes with multiple external fins. However, they used an iterative procedure to find the prespecified fluxes and did not extend the method to two-dimensional fins as we have done in Model 4.

The steady-state temperature distribution in the tube is governed by Laplace's equation

$$\frac{1}{r}\frac{\partial}{\partial r}\left(r\frac{\partial T_t}{\partial r}\right)+\frac{1}{r^2}\frac{\partial^2 T_t}{\partial \theta^2}=0 \tag{16}$$

subject to the boundary conditions:

$$\frac{\partial T_t}{\partial \theta}=0 \qquad \text{at } \theta=0,\ \alpha\leqslant r\leqslant 1 \tag{17a}$$

$$\frac{\partial T_t}{\partial \theta}=0 \qquad \text{at } \theta=\pi,\ \alpha\leqslant r\leqslant 1 \tag{17b}$$

$$\frac{\partial T_t}{\partial r}=\delta Bi\, T_t \qquad \text{at } 0\leqslant\theta\leqslant\pi,\ r=\alpha \tag{17c}$$

$$\begin{aligned}\frac{\partial T_t}{\partial r}=q(\theta)&=0 \quad \text{at } 0\leqslant\theta\leqslant\omega,\ r=1\\ &=q_f \quad \text{at } \omega\leqslant\theta\leqslant\omega+\phi,\ r=1\\ &=q_e \quad \text{at } \omega+\phi\leqslant\theta\leqslant\pi,\ r=1.\end{aligned} \tag{17d}$$

Equation (16), subject to boundary conditions (17a)–(17d), can be solved by a separation-of-variables technique to obtain

$$\begin{aligned}T_t(r,\theta)=&\left(\frac{\phi}{\pi}q_f+\frac{\omega}{\pi}q_e\right)\left(\ln\frac{r}{\alpha}+\frac{1}{\alpha\delta\, Bi}\right)\\&-\sum_{n=1}^{\infty}\frac{2\cos(n\theta)}{\pi n^3}\left[\{\sin[n(\omega+\phi)]-\sin(n\omega)\}q_f\right.\\&\left.-\sin[n(\omega+\phi)]q_e\right]\left\{\frac{(n-\alpha\delta\, Bi)\alpha^{2n}r^{-n}+(n+\alpha\delta\, Bi)r^n}{(n-\alpha\delta\, Bi)\alpha^{2n}-(n+\alpha\delta\, Bi)}\right\}.\end{aligned} \tag{18}$$

Because the average fluxes entering and leaving the finned and exposed tube surfaces must be the same, q_f and q_e are related to the average temperatures, $\bar{T}_{tfo}$ and $\bar{T}_{teo}$, of these two surfaces by

$$\begin{aligned}q_f=\kappa\, Bi(1-\bar{T}_{tfo})&=\kappa\, Bi\left[1-\frac{1}{\phi}\int_{\omega}^{\omega+\phi}T_t(1,\theta)\,d\theta\right]\\&=\kappa\, Bi\left[1+\left(\frac{\phi A}{\pi}+\frac{2S_1}{\phi}\right)q_f+\left(\frac{\omega A}{\pi}-\frac{S_1}{\phi}\right)q_e\right]\end{aligned} \tag{19}$$

and

$$\begin{aligned}q_e=Bi(1-\bar{T}_{teo})&=Bi\left[1-\frac{1}{\omega}\int_{\omega+\phi}^{\pi}T_t(1,\theta)\,d\theta\right]\\&=Bi\left[1+\left(\frac{\phi A}{\pi}-\frac{S_1}{\omega}\right)q_f+\left(\frac{\omega A}{\pi}+\frac{S_2}{\omega}\right)q_e\right]\end{aligned} \tag{20}$$

where

$$\begin{aligned}A&=\ln\alpha-\frac{1}{\alpha\delta\, Bi},\quad S_1=\sum_{n=2,4,\ldots}^{\infty}\frac{4\Lambda_n}{\pi n^3}\sin^2(n\omega)\\S_2&=\sum_{n=1}^{\infty}\frac{2\Lambda_n}{\pi n^3}\sin^2(n\omega)\\\Lambda_n&=\frac{(n-\alpha\delta\, Bi)\alpha^{2n}+(n+\alpha\delta\, Bi)}{(n-\alpha\delta\, Bi)\alpha^{2n}-(n+\alpha\delta\, Bi)}.\end{aligned} \tag{21}$$

Equations (19) and (20) are linear simultaneous equations which can be readily solved for q_f and q_e. If we let

$$\begin{aligned}a_{11}&=\frac{1}{\kappa\, Bi}-\frac{\phi A}{\pi}-\frac{2S_1}{\phi},\quad a_{12}=-\frac{\omega A}{\pi}+\frac{S_1}{\phi}\\a_{21}&=-\frac{\phi A}{\pi}+\frac{S_1}{\omega},\quad a_{22}=\frac{1}{Bi}-\frac{\omega A}{\pi}-\frac{S_2}{\omega}\end{aligned} \tag{22}$$

then

$$q_f=\frac{a_{22}-a_{12}}{a_{11}a_{22}-a_{12}a_{21}},\quad q_e=\frac{a_{11}-a_{21}}{a_{11}a_{22}-a_{12}a_{21}}. \tag{23}$$

The overall heat transfer coefficient can now be determined directly from q_f and q_e as

$$\frac{U_0R_0}{k_t}=\frac{\phi}{1+\gamma}q_f+\frac{\omega}{1+\gamma}q_e. \tag{24}$$

Model 4. Tube-two-dimensional, fin-two-dimensional model

Model 4 is similar to Model 3 except that it relaxes the assumption of one-dimensional conduction in the membrane fin. To solve this two-dimensional problem, it is convenient to retain the assumptions that the fin is rectangular and that the temperature of its base is constant and equal to the average temperature, $\bar{T}_{tfo}$, of the finned portion of the tube outer surface. The resulting solution provides a more accurate value of κ (i.e. h_f/h_o) than the one-dimensional approximation used for Model 3.

The steady-state temperature distribution in the half-fin is also described by Laplace's equation which, in Cartesian coordinates, reads

$$\frac{\partial^2 T_f}{\partial x^2} + \frac{\partial^2 T_f}{\partial y^2} = 0. \tag{25}$$

The boundary conditions are

$$T_f = \bar{T}_{tfo} \qquad \text{at } x = 0, 0 \leqslant y \leqslant 2\beta \tag{26a}$$

$$\frac{\partial T_f}{\partial x} = 0 \qquad \text{at } x = \gamma, 0 \leqslant y \leqslant 2\beta \tag{26b}$$

$$\frac{\partial T_f}{\partial y} = 0 \qquad \text{at } 0 \leqslant x \leqslant \gamma, y = 0 \tag{26c}$$

$$\frac{\partial T_f}{\partial y} = \frac{Bi}{\varepsilon}(1 - T_f) \qquad \text{at } 0 \leqslant x \leqslant \gamma, y = 2\beta. \tag{26d}$$

The solution which satisfies equations (25) and (26a)–(26d) is

$$T_f(x, y) = 1 - Bi(1 - \bar{T}_{tfo}) \times \sum_{n=1}^{\infty} \left\{ \frac{2 \sin(2\lambda_n \beta) \cos(\lambda_n y)}{\varepsilon \lambda_n \left[\sin^2(2\lambda_n \beta) + \frac{2\beta\, Bi}{\varepsilon} \right]} \times [\cosh(\lambda_n x) - \tanh(\lambda_n \gamma) \sinh(\lambda_n x)] \right\} \tag{27}$$

where the eigenvalues, λ_n, are the roots of

$$\lambda \tanh(2\lambda\beta) - \frac{Bi}{\varepsilon} = 0. \tag{28}$$

The nth eigenvalue lies between $(n-1)\pi/2\beta$ and $(n-1/2)\pi/2\beta$; as n becomes larger, the roots approach the latter discontinuity.

The average heat flux over the tube–fin interface is therefore given by

$$q_f = \frac{1}{\phi} \int_{\omega}^{\omega+\phi} \varepsilon \left. \frac{\partial T_f}{\partial x} \right|_{x=0} d\theta \simeq \frac{\varepsilon}{2\beta} \int_0^{2\beta} \left. \frac{\partial T_f}{\partial x} \right|_{x=0} dy$$

$$= Bi(1 - \bar{T}_{tfo}) \sum_{n=1}^{\infty} \frac{\sin^2(2\lambda_n \beta) \tanh(\lambda_n \gamma)}{\beta \lambda_n \left[\sin^2(2\lambda_n \beta) + \frac{2\beta\, Bi}{\varepsilon} \right]}. \tag{29}$$

When equation (29) is compared with the first equality in equation (19), it is apparent that

$$\kappa = \sum_{n=1}^{\infty} \frac{\sin^2(2\lambda_n \beta) \tanh(\lambda_n \gamma)}{\beta \lambda_n \left[\sin^2(2\lambda_n \beta) + \frac{2\beta\, Bi}{\varepsilon} \right]}. \tag{30}$$

This improved expression for κ can be substituted into equation (22) to obtain the Model 4 values of q_f, q_e and $U_0 R_o / k_t$.

Model 5. Numerical finite difference model

Model 5 employs a finite difference method to solve the membrane wall heat transfer problem which results when all the special assumptions of Models 1–4 are relaxed. In this case, the half-tube and half-fin are treated as separate two-dimensional conductors with the proviso that local temperatures and fluxes must match at their mutual boundary.

To accommodate its curved surface, the non-rectangular fin (in x, y coordinates) was first mapped into a unit square (in transformed ξ, η coordinates) using the weak constraint numerical grid generation method developed by Ryskin and Leal [13]. This numerical transformation method not only produces an orthogonal grid but also, because the locations of the boundary nodes can be specified beforehand, provides a convenient way to match boundary conditions in multi-domain problems. The two elliptic partial differential equations for x and y in terms of ξ and η, subject to appropriate Dirichlet and Neumann boundary conditions, are solved using the finite difference method. The transformed grid was taken to be uniform in both coordinate directions, and second-order accurate difference approximations were employed at every node. The resulting set of algebraic equations was solved iteratively by line over-relaxation until the maximum absolute change in x and y was less than 10^{-5}. The cylindrical grid in the tube section was made nonuniform in the θ-direction to provide a greater concentration of nodes near the fin.

In Model 5, the temperature distribution in the tube wall is once again governed by equation (16) subject to boundary conditions (17a)–(17c) and

$$\frac{\partial T_t}{\partial r} = \begin{cases} 0 & \text{at } 0 \leqslant \theta \leqslant \omega, r = 1 \\ Bi(1 - T_t) & \text{at } \omega + \phi \leqslant \theta \leqslant \pi, r = 1. \end{cases} \tag{31}$$

The fin problem in transformed coordinates becomes

$$\frac{\partial}{\partial \xi}\left(\frac{h_\eta}{h_\xi} \frac{\partial T_f}{\partial \xi} \right) + \frac{\partial}{\partial \eta}\left(\frac{h_\xi}{h_\eta} \frac{\partial T_f}{\partial \eta} \right) = 0 \tag{32}$$

with

$$\frac{\partial T_f}{\partial \eta} = 0 \qquad \text{at } \eta = 0, 0 \leqslant \xi \leqslant 1$$

$$\frac{\partial T_f}{\partial \eta} = \frac{h_\eta}{\varepsilon} Bi(1 - T_f) \qquad \text{at } \eta = 1, 0 \leqslant \xi \leqslant 1$$

$$\frac{\partial T_f}{\partial \xi} = 0 \qquad \text{at } 0 \leqslant \eta \leqslant 1, \xi = 1. \tag{33}$$

The metrics h_ξ and h_η of the coordinate transformation are defined by

$$h_\xi = [(\partial x/\partial \xi)^2 + (\partial y/\partial \xi)^2]^{1/2}$$

$$\text{and} \quad h_\eta = [(\partial x/\partial \eta)^2 + (\partial y/\partial \eta)^2]^{1/2} \tag{34}$$

and can be estimated, where necessary, by numerically differentiating the grid solution. In the weak constraint method of Ryskin and Leal, the scale factors, h_η/h_ξ and h_ξ/h_η, are, in general, calculated for the whole domain from preassigned corner values using a simple interpolation formula. The matching conditions which complete the specification of the problem are

$$T_t = T_f \qquad \text{at } \omega \leqslant \theta \leqslant \omega + \phi, r = 1$$

$$\frac{\partial T_t}{\partial r} = \frac{\varepsilon}{h_\xi} \frac{\partial T_f}{\partial \xi} \qquad 0 \leqslant \eta \leqslant 1, \xi = 0. \tag{35}$$

In practice, a special finite difference form of Laplace's equation was devised for the nodes on the fin–tube junction. These expressions, which inherently satisfy equation (35), allowed the entire assembly to be treated as a single domain during the solution procedure.

Equations (16) and (32) were discretized using the control volume approach recommended by Patankar [14]. The boundary conditions, all of which involve normal derivatives, were assigned using 'fictitious' points located outside the solution domain. The nodal temperatures in the half-tube and half-fin were initialized by means of equations (18) and (27), respectively, employing the values of q_f and q_c obtained from Model 4. The solution was then progressed iteratively using a line over-relaxation procedure until the maximum absolute temperature change was less than 10^{-5}. After convergence was attained, the overall heat transfer rates and coefficients were calculated using the heat transfer conditions existing at the exposed inner and outer boundaries. These two estimates were always found to agree to within six significant figures indicating that the discretization method was not only locally, but also globally, conservative.

The accuracy of the numerical solution was assessed by examining the behaviour of individual temperature values and the overall heat transfer coefficient as the grids were made progressively finer for three widely different sets of conditions. On the basis of this analysis, it is estimated that all U_0R_o/k_t values reported for Model 5 are accurate to at least three and usually four significant figures.

RESULTS AND DISCUSSION

Membrane waterwalls for fluidized bed furnaces are typically constructed from carbon steel components. The tubes have diameters ranging from 32 to 60 mm and wall thicknesses of 3–6 mm depending on the diameter and the water-side pressure. The membranes which interconnect the tubes commonly have half-widths in the range of 12–30 mm and thicknesses of 6–12 mm [15]. Furnace-side heat transfer coefficients are normally about 200–300 W m^{-2} K^{-1} for fluidized bed boilers but may be as low as 100 W m^{-2} K^{-1} for circulating bed boilers under reduced load conditions [6]. Water-side coefficients vary from about 1000 (non-boiling service) to 6000 W m^{-2} K^{-1} (nucleate boiling) [5]. These approximate limiting conditions yield the typical industrial dimensionless parameter ranges listed in Table 1. Based on these limits, the following standard set of parameters was selected: $\alpha = 0.8$, $\beta = 0.15$, $\gamma = 1.0$, $\delta = 10.0$, $\varepsilon = 1.0$ and $Bi = 1.0$. From this base case set, each parameter was varied in turn through the broad range of discrete values shown in Table 1. The only exception to this procedure was for α and β, the values of which were altered in unison to simulate a transition from two-dimensional to one-dimensional conduction in the tube and the fin. The parameter ranges investigated not only span the region of practical interest but also include more extreme cases to help clarify or explain various trends which were observed.

For each set of parameters investigated, the following heat transfer characteristics were extracted for comparison from all five models: the overall heat transfer coefficient, U_0R_o/k_t, the enhancement ratio, E, the heat transfer rates, $\hat{q}_c$ and $\hat{q}_f$, through the exposed tube surface and the fin, respectively, and the average heat fluxes, q_c and q_f, at the exposed surface and the fin–tube junction, respectively. To further assist the interpretation of the results, average interface temperatures and, where possible, local interface temperatures and heat fluxes were also calculated. Finally, in the case of Model 5, the nodal temperatures in the fin and the tube were superimposed on the outline of the assembly as a set of isothermal contour lines.

As an example, consider the results obtained with the base case conditions. The finite difference grid used for Model 5 is illustrated in Fig. 3(a). Because the angle subtended by the fin base is fairly acute in this instance, the numerically-generated orthogonal grid in the fin is only marginally distorted from a Cartesian grid. The grid lines are purposely spread out with distance from the fin–tube junction because the fin tip contributes only minimally to the overall heat transfer.

Figure 3(b) shows the Model 5 temperature contours for this case. This figure illustrates clearly the rationale used in developing Model 2. While conduction is primarily radial in the exposed portion of

Table 1. Dimensionless parameter ranges and values investigated. Underlined figures are base case values. Other cases were investigated by changing one parameter at a time or by varying α and β together in vertical pairs

Dimensionless variable	Typical industrial range	Values investigated
$\alpha(R_i/R_o)$	0.6–0.9	0.5, 0.7, <u>0.8</u>, 0.9, 0.85, 0.99
$\beta(t/R_o)$	0.1–0.3	0.25, 0.2, <u>0.15</u>, 0.1, 0.05, 0.01
$\gamma(w/R_o)$	0.4–2.0	0.2, <u>1.0</u>, 5.0
$\delta(h_i/h_o)$	3–60	0.1, 1.0, <u>10.0</u>, 100.0, 1000.0
$\varepsilon(k_t/k_w)$	1.0	0.01, 0.1, <u>1.0</u>, 10.0, 100.0
$Bi(h_oR_o/k_t)$	0.04–1.0	0.01, 0.1, <u>1.0</u>, 10.0, 100.0

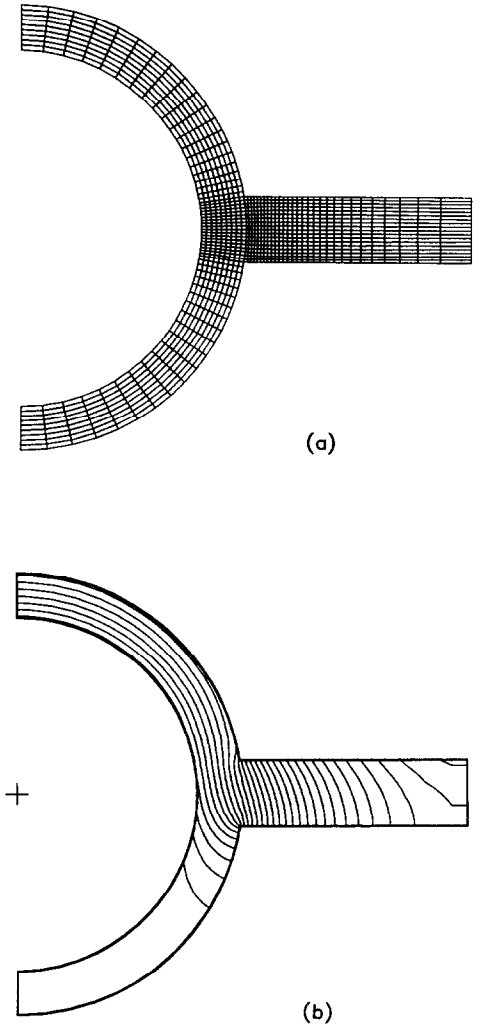

FIG. 3. (a) Grid pattern used to obtain finite difference solution for base case conditions specified in Table 1. (b) Isotherm contours for base case predicted by Model 5, minimum = 0.025 (increment = 0.025) maximum = 0.775.

the tube, it is mostly tangential in the insulated section. In the fin, conduction occurs predominantly in the width-wise direction but becomes two-dimensional near the tip because of the symmetry condition there. Since the heat flux vector must be orthogonal to the isotherms, it is apparent that all of the energy dissipated through the insulated tube wall is drawn from the fin. In fact, the fin is such an effective conduit that it also supplies some heat to the exposed tube section. As a consequence, the average temperature at the fin junction is significantly higher than that of the exposed tube surface, giving credibility to the idea of treating the finned and exposed tube sections as separate one-dimensional pathways.

Figure 4 compares, for the base case conditions, the temperature and heat flux distributions predicted by Models 1, 2, 4 and 5 for the inner (a) and outer (b) surfaces of the half-tube. The results of Model 3 are not included because with the exception of a constant heat flux at the fin–tube junction, they differ almost imperceptibly from those of Model 4. The heat transfer characteristics obtained from all five models for this case are presented in the top five rows of Table 2.

Figure 4 demonstrates why, as revealed in Table 2, the more sophisticated analytical models, Models 2–4, yield more accurate heat transfer estimates than the simple one-dimensional Model 1. Because it permits only radial conduction in the tube, Model 1 requires that the inner and outer tube surfaces each be isothermal. Thus, even though these constant temperatures are reasonably representative of their true average values, the model, by necessity, overpredicts the rates of heat transfer into the exposed section of the tube and out of the insulated portion. The net result is an estimate of the overall heat transfer coefficient which exceeds the exact value by 13.4%.

Model 2 provides an improved representation of the temperature and heat flux distributions particularly in the insulated tube section where the more realistic assumption of tangential conduction is made. The predicted temperature profile in this section is approximately equal to the mean of the actual inner and outer surface distributions. As a consequence, Model 2 overestimates the rate of heat dissipation from the inner surface as well as the rate of transfer through the fin, which acts as the sole supplier to this section of the tube. Because it treats the exposed tube portion as a one-dimensional radial resistor and therefore cannot account for the outer surface temperature rise near the base of the fin, the second model also slightly exaggerates the heat transfer rate through this section. Nonetheless, Model 2 provides remarkably accurate estimates of all of the heat transfer characteristics.

In the case of Model 4, the temperature and inner surface heat flux profiles plotted in Fig. 4(a) were obtained from the tube wall solution. The outer surface heat flux distributions in Fig. 4(b) were derived from the local temperature and the convection boundary condition for the exposed portion, and from the local temperature gradients within the fin for the finned portion. Of course, the heat flux must be identically zero over the outer surface of the insulated tube section. For the most part, the temperature and heat flux distributions predicted by the fully two-dimensional Model 4 are indistinguishable from the exact results of Model 5. The noticeable differences that occur at the fin–tube interface are easily reconciled since Model 4 requires that the temperatures and fluxes at this boundary match only on an average rather than a local basis. As Table 2 reveals, the agreement between Models 4 and 5 for the base case carries over to the calculated heat transfer characteristics where, for example, the discrepancy in the overall heat transfer coefficient is now only about 0.1%.

The comparative trends between the models are similar for all of the cases investigated. Table 2 lists the results calculated by the five models for selected conditions straddling the base case values. The mini-

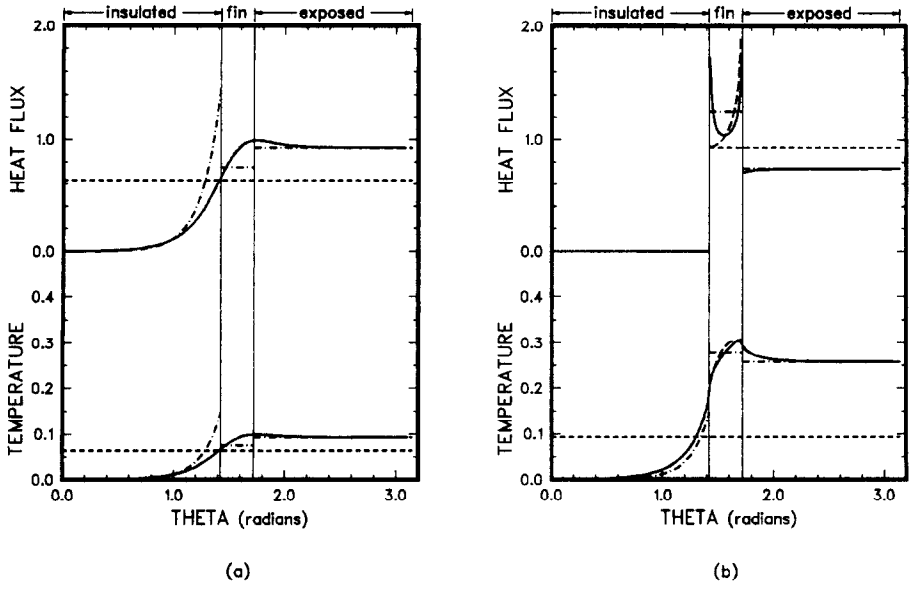

FIG. 4. Dimensionless temperature and heat flux profiles for the base case conditions specified in Table 1: (a) along inside surface of tube; (b) along outside surface of tube; --------, Model 1; - · - · - · -, Model 2; — — — —, Model 4; ———, Model 5.

mum, maximum and average absolute errors attributable to each model for all 20 sets of conditions delineated in Table 1 are compiled in Table 3.

The latter table demonstrates the same general improvement with increasing model sophistication as for the base case. Except for the unrealistic condition, $Bi = 100$, the overall heat transfer coefficients predicted by Model 4 all lie within 0.7% of their exact values. This exceptional performance, however, must be weighed against the calculational requirements of Model 4 (root-solving for a set of eigenvalues plus the evaluation of three infinite series). More notable perhaps is the predictive ability of Model 2 which, although simple to use and empirical in nature, provides remarkably accurate (<2% average deviation) estimates of U_0R_o/k_t. Model 3 represents a reasonable compromise; it is more reliable than Model 2 yet, because it requires the evaluation of only two very similar series, is not as computationally intensive as Model 4. As expected, those models (Models 2–4) which, to a greater or lesser extent, account for two-dimensional conduction in the tube wall, yield much better estimates of $\hat{q}_c$ than the fully one-dimensional Model 1. However, only Model 4, which allows for two-dimensional conduction in the fin as well as the tube, provides consistently adequate predictions of $\hat{q}_f$.

Other, more specific trends in the predictive performance of the various models are discernible upon closer inspection of Table 2. For example, as the tube wall and fin thicknesses are simultaneously diminished (conferring a greater degree of one-dimensionality to the transfer paths), all four approximate models give improved estimates of U_0R_o/k_t, $\hat{q}_c$ and $\hat{q}_f$. The single exception is Model 1 which consistently overpredicts the rate of heat transfer along the fin. As α and β are reduced, the heat flux q_f rises more precipitously than q_c (Table 2), increasing the tube wall temperature near the base of the fin to values far above that of the exposed tube surface. Thus, since the average temperature for the outer tube surface used by Model 1 will be lower than the true temperature at the fin–tube junction, $\hat{q}_f$ is always exaggerated.

When the fin conductivity is much less than that of the tube (e.g. $\varepsilon = 0.1$), $\hat{q}_f$ is greatly overestimated by all three models which assume one-dimensional conduction in the fin. At higher conductivity ratios, Models 2 and 3 yield much better predictions of this quantity. The fully two-dimensional Model 4 provides acceptable answers for all values of ε. These trends can be rationalized by examining the temperature contour plots for $\varepsilon = 0.1$ (Fig. 5(c)) and $\varepsilon = 10.0$ (Fig. 5(d)). At $\varepsilon = 0.1$, most of the heat transferred from the fin is collected near the junction of the exposed surfaces making conduction in the fin conspicuously two-dimensional. Since the actual fin surface temperatures rise much more rapidly from the junction than can be predicted by a one-dimensional model with the same base temperature, Models 1–3 experience abnormally high convection rates and hence overpredict $\hat{q}_f$. As ε is increased, heat conduction in the fin becomes more one-dimensional because of the greater uniformity of the base temperature and the relatively greater significance of the convection resistance along its exposed surface. Thus, when $\varepsilon = 10.0$, Models 2 and 3 both give $\hat{q}_f$ predictions which compare well with the results of Models 4 and 5. However, again because rapid heat transfer through the fin raises its base temperature above the average outer tube surface tem-

Table 2. Comparison of membrane wall heat transfer models for representative values of the dimensionless parameters[a]. Values shown in parentheses are percent deviations from the exact (Model 5) predictions

Parameters[a]	Model	U_0R_o/k_t	$\hat{q}_e$	$\hat{q}_f$	E	q_c	q_f
	1	0.799 (13.4)	1.169 (11.5)	0.430 (19.1)	1.372	0.823	1.426
	2	0.715 (1.5)	1.054 (0.5)	0.377 (4.4)	1.228	0.742	1.251
Base case	3	0.710 (0.8)	1.049(−0.0)	0.372 (3.0)	1.219	0.738	1.234
	4	0.704(−0.1)	1.049 (0.1)	0.359(−0.6)	1.208	0.739	1.190
	5	0.705 (—)	1.049 (—)	0.361 (—)	1.210	0.738	1.198
	1	0.628 (18.4)	0.848 (19.6)	0.408 (15.9)	1.514	0.643	0.808
	2	0.547 (3.0)	0.696(−1.8)	0.397 (12.7)	1.317	0.528	0.785
$\alpha = 0.50, \beta = 0.25$	3	0.539 (1.5)	0.706(−0.4)	0.371 (5.5)	1.298	0.536	0.735
	4	0.530(−0.1)	0.709 (0.0)	0.350(−0.5)	1.277	0.538	0.693
	5	0.531 (—)	0.709 (—)	0.352 (—)	1.279	0.538	0.697
	1	0.841 (8.2)	1.393 (6.3)	0.289 (18.7)	1.239	0.916	2.887
	2	0.779 (0.3)	1.315 (0.3)	0.243 (0.0)	1.247	0.865	2.432
$\alpha = 0.95, \beta = 0.05$	3	0.778 (0.2)	1.310(−0.0)	0.246 (1.2)	1.146	0.862	2.461
	4	0.777(−0.0)	1.311(−0.0)	0.243(−0.0)	1.144	0.862	2.431
	5	0.777 (—)	1.311 (—)	0.243 (—)	1.144	0.862	2.432
	1	1.140 (11.9)	1.205 (13.5)	0.163 (0.9)	1.174	0.848	0.542
	2	1.018(−0.1)	1.054(−0.7)	0.168 (4.1)	1.049	0.742	0.559
$\gamma = 0.20$	3	1.019 (0.0)	1.062 (0.0)	0.162(−0.1)	1.050	0.747	0.536
	4	1.013(−0.6)	1.062 (0.1)	0.153(−5.4)	1.043	0.748	0.508
	5	1.019 (—)	1.061 (—)	0.162 (—)	1.050	0.747	0.537
	1	0.270 (13.8)	1.166 (11.2)	0.451 (21.2)	1.388	0.821	1.499
	2	0.241 (1.7)	1.054 (0.5)	0.391 (5.0)	1.240	0.742	1.299
$\gamma = 5.0$	3	0.239 (1.0)	1.048(−0.0)	0.387 (3.8)	1.231	0.738	1.283
	4	0.237 (0.2)	1.048 (0.0)	0.376 (0.9)	1.222	0.738	1.247
	5	0.237 (—)	1.048 (—)	0.372 (—)	1.219	0.738	1.236
	1	0.508 (23.5)	0.743 (26.3)	0.273 (16.5)	1.600	0.523	0.907
	2	0.418 (1.5)	0.574(−2.4)	0.261 (11.3)	1.315	0.404	0.866
$\delta = 1.0$	3	0.413 (0.5)	0.584(−0.7)	0.243 (3.4)	1.302	0.411	0.805
	4	0.411(−0.2)	0.586(−0.4)	0.236(−0.4)	1.293	0.413	0.782
	5	0.412 (—)	0.589 (—)	0.234 (—)	1.296	0.414	0.778
	1	0.848 (10.6)	1.240 (8.3)	0.456 (17.3)	1.334	0.873	1.153
	2	0.781 (1.9)	1.149 (0.4)	0.413 (6.4)	1.229	0.809	1.373
$\delta = 100$	3	0.773 (0.8)	1.145 (0.0)	0.401 (3.1)	1.216	0.806	1.330
	4	0.766(−0.1)	1.146 (0.1)	0.386(−0.7)	1.205	0.807	1.281
	5	0.767 (—)	1.145 (—)	0.388 (—)	1.206	0.806	1.290
	1	0.677 (14.5)	1.207 (13.5)	0.148 (22.9)	1.163	0.850	0.491
	2	0.604 (2.1)	1.054(−0.9)	0.154 (28.2)	1.036	0.742	0.512
$\varepsilon = 0.10$	3	0.605 (2.3)	1.062(−0.1)	0.148 (22.7)	1.038	0.748	0.490
	4	0.592 (0.1)	1.064 (0.1)	0.121 (0.3)	1.017	0.749	0.400
	5	0.592 (—)	1.063 (—)	0.120 (—)	1.016	0.749	0.399
	1	0.925 (16.1)	1.129 (8.8)	0.720 (29.7)	1.587	0.795	2.390
	2	0.798 (0.2)	1.054 (1.5)	0.543(−2.3)	1.370	0.742	1.802
$\varepsilon = 10.0$	3	0.793(−0.5)	1.038(−0.0)	0.548(−1.3)	1.361	0.731	1.819
	4	0.791(−0.7)	1.038 (0.0)	0.545(−1.9)	1.358	0.731	1.809
	5	0.797 (—)	1.038 (—)	0.555 (—)	1.367	0.731	1.843
	1	0.105 (4.5)	0.128 (4.1)	0.082 (5.0)	1.532	0.090	0.271
	2	0.101 (0.1)	0.124 (0.6)	0.077(−0.7)	1.468	0.087	0.256
$Bi = 0.10$	3	0.100(−0.2)	0.123(−0.0)	0.077(−0.6)	1.463	0.087	0.256
	4	0.100(−0.5)	0.123 (0.0)	0.077(−1.3)	1.459	0.087	0.255
	5	0.100 (—)	0.123 (—)	0.078 (—)	1.466	0.087	0.258
	1	3.630 (46.3)	6.468 (51.2)	0.792 (15.7)	1.551	4.554	2.629
	2	2.579 (3.9)	4.231(−1.1)	0.927 (35.5)	1.102	2.979	3.080
$Bi = 10.0$	3	2.537 (2.2)	4.260(−0.4)	0.814 (18.9)	1.084	3.000	2.703
	4	2.495 (0.6)	4.273(−0.1)	0.718 (4.9)	1.066	3.009	2.383
	5	2.482 (—)	4.279 (—)	0.685 (—)	1.061	3.013	2.273

[a] Values are listed only where they differ from the base case values identified in Table 1.

Table 3. Overall comparison of waterwall model errors for the 20 cases identified in Table 1

Heat transfer characteristic	Model	Error		
		Minimum	Maximum	Average
$U_0 R_o/k_t$	1	4.46	82.82	18.57
	2	−0.14	10.67	1.89
	3	−0.48	5.06	1.11
	4	−0.65	1.80	0.33
	5	0.0	0.0	0.0
$\hat{q}_c$	1	4.09	98.44	19.39
	2	−18.16	1.51	1.89
	3	−3.90	0.04	0.43
	4	−3.09	0.11	0.29
	5	0.0	0.0	0.0
$\hat{q}_f$	1	−39.74	102.49	23.06
	2	−2.60	126.40	22.45
	3	−1.35	113.88	14.11
	4	−5.38	23.42	3.10
	5	0.0	0.0	0.0

perature, Model 1 continues to seriously overestimate $\hat{q}_f$.

Similar trends are observed for similar reasons when the tube Biot number (and hence fin Biot number, $\beta\, Bi/\varepsilon$) is varied from its standard value. As shown by Figs. 5(e) and (f), when Bi is raised from 0.1 and 10.0, the heat flow pattern in the fin changes from mostly one-dimensional to predominantly two-dimensional. As a result, Models 2 and 3 overpredict $\hat{q}_f$ at $Bi = 10.0$ but yield reasonable estimates at $Bi = 0.1$.

The heat transfer characteristics listed in Table 2 also point out several trends which bear consideration in the design of membrane waterwalls.

Effect of tube and fin thickness

Decreasing the tube wall thickness increases the total heat transfer rate through the assembly because the wall offers less radial resistance in the exposed

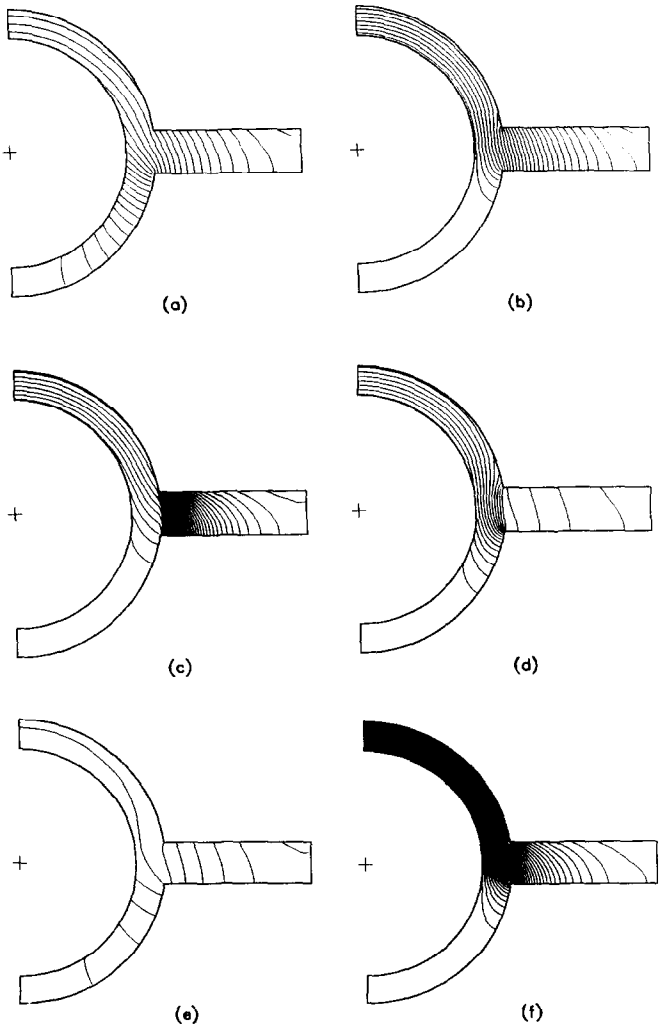

FIG. 5. Isotherm contours provided by Model 5 for representative cases with dimensionless parameters changed from their base case values: (a) $\delta = 1.0$, minimum = 0.075 (increment = 0.025) maximum = 0.850; (b) $\delta = 100.0$, 0.025 (0.025) 0.750; (c) $\varepsilon = 0.1$ (0.025) 0.75; (d) $\varepsilon = 10.0$, 0.025 (0.025) 0.475; (e) $Bi = 0.1$, 0.025 (0.025) 0.275; (f) $Bi = 10.0$, 0.025 (0.025) 0.975.

tube sector. However, this augmentation of U_0R_o/k_t is not reflected in the enhancement ratio, E, especially if the fin thickness is simultaneously diminished. When α is increased and β is reduced, the cross-sectional areas in the dominant conduction directions (tangential in the insulated tube sector, width-wise in the fin) are decreased and the contribution by these two components to the overall transfer is significantly lessened. For example, when $\alpha = 0.5$ and $\beta = 0.25$ the heat transfer flux from the inside surface of the tube at $\theta = 0$ is more than 15% of its maximum value at $\theta = \pi$. On the other hand, when $\alpha = 0.95$ and $\beta = 0.05$, the inside flux is essentially zero over the lower 60% of the insulated sector. These results underline the importance of the membrane fin and of the insulated portion of the tube in augmenting heat transfer to membrane waterwalls. Because the heat dissipated by the latter is almost invariably collected by the former, these two components play an important, synergistic role in the overall process.

Effect of fin width

As might be expected, an increase in γ has little effect on the rate of heat transfer through the exposed tube section but, because the area available for convection is magnified, it enhances transfer through the fin and consequently increases the enhancement ratio of the assembly. However, this improvement in performance does not continue indefinitely; for dimensionless distances from the fin base exceeding 2, the fin becomes essentially isothermal at the furnace-side temperature and $\hat{q}_f$ and E approach asymptotic maxima. Of course, because projected area is used in the definition of the overall heat transfer coefficient, $U_0R_o/k_t \to 0$ as $\gamma \to \infty$. Thus, for most conditions of industrial interest, maximum heat transfer per unit area of waterwall is obtained when $\gamma = 0$. However, a non-zero membrane width may be required to allow easier fabrication, to ensure effective convection over the entire exposed surface and to prevent particles from lodging in the gap between tubes.

Effect of inside heat transfer coefficients

As δ is increased, Table 2 reveals two notable trends. First, the overall heat transfer rate tends to increase as for an unfinned, uninsulated tube. As $\delta \to 0$, the inside convection resistance becomes dominant and the overall rate falls to zero; as $\delta \to \infty$, the inside resistance becomes negligible and U_0R_o/k_t asymptotically approaches a maximum. Secondly, the enhancement ratio, E, falls monotonically from a high value when δ is small to an asymptotic minimum when δ becomes very large. This is the reverse of what would be anticipated for an externally-finned tube where the enhancement in heat transfer is a maximum when the outside convection resistance dominates (i.e. when $\delta \gg 1$). Figures 5(a) and (b) reveal why membrane walls do not behave in the expected manner. When the inside convection resistance is significant (e.g. at $\delta = 1.0$), a strong angular temperature gradient is created in the insulated portion of the tube wall. Consequently, a substantial fraction of the energy entering the inside fluid is transmitted by this insulated section, leading to an overall augmentation of the heat transfer rate. Conversely, when the inside resistance is relatively small (e.g. at $\delta = 100$), the entire inside surface of the tube is approximately isothermal and the potential for angular conduction in the insulated section is greatly diminished. These results again demonstrate the importance of this portion of the tube in assisting waterwall heat transfer.

Effect of fin thermal conductivity

As ε is increased, heat collection by the fin contributes more strongly to the overall heat transfer. For example, when ε is raised from 0.1 to 10.0 (Table 2), the heat transfer rate through the exposed tube surface declines slightly while the rate through the fin increases nearly five-fold causing a 35% improvement in the overall heat transfer coefficient. For $\varepsilon \ll 1$ and $\varepsilon \gg 1$, U_0R_o/k_t approaches separate asymptotic values. The former corresponds to the case where the fin acts to insulate an additional portion of the tube surface allowing heat to be transferred at a reduced rate through the exposed tube surface only. When $\varepsilon = 0.1$, for example, the enhancement ratio falls to its lowest value in Table 2, underscoring once again the co-operative role played by the fin and the insulated tube section in waterwall heat transfer. For large ε, the conduction resistance in the fin becomes negligible compared to the convection resistance at its exposed surface, and h_f/h_o (from equation (6) or (30)) approaches the ratio of the exposed surface area to the basal area (i.e. $\kappa \to \gamma/2\beta \simeq \gamma/\phi$). If the outer tube surface temperature were constant for $\omega \leqslant \theta \leqslant \pi$, then it is straightforward to prove that the maximum theoretical enhancement is $E = 2(\omega+\gamma)/\pi$ or 1.54 at the standard conditions. However, this maximum value can never be achieved in practice because the rapid transfer of heat through the highly conductive fin raises its base temperature to values well above the exposed surface temperature of the tube.

Effect of outside Biot number

As Bi is increased, the overall heat transfer coefficient rises, the enhancement ratio falls and the fin plays a diminishing role in the overall transfer process. When Bi is very small (with δ fixed), the inside and furnace-side resistances dominate to such an extent that the entire assembly is almost isothermal. As a consequence, the heat fluxes along the inner and outer exposed surfaces are essentially constant leading to maximal augmentation. When Bi is very large, the inside and furnace-side resistances are both negligible, the dimensionless temperatures at the inside surface of the tube and the outside surfaces of both the fin and the tube approach 0 and 1, respectively, and heat transfer is controlled entirely by the lengths of the conduction paths within the assembly. Thus, most of the heat is transferred across the exposed portion of

the tube wall while the fin and the insulated section play only a minor role in the overall process. In fluidized bed boilers, although attempts are made to maintain the furnace-side heat transfer coefficients as large as possible, Biot numbers rarely exceed unity.

CONCLUSIONS

(1) Four approximate models are derived for heat conduction in membrane waterwalls for the case where heat transfer coefficients are uniform both inside the tubes and on the exposed outer (furnace-side) surface of the tubes and connecting fins. These models vary in complexity from a one-dimensional electrical resistance analogue to one which allows fully two-dimensional temperature variation in both the tube and the fin, with matching average temperatures and fluxes at the exposed outer tube surface and the fin–tube boundary.

(2) Predictions from the four approximate models are compared with exact values obtained from a numerical finite difference solution of Laplace's equation subject to the appropriate boundary conditions including matching local temperatures and fluxes at the mutual boundary between the fin and the tube. A cylindrical polar grid is used in the tube while a numerically-generated orthogonal grid is employed in the fin to accommodate the curved fin–tube interface.

(3) Except for the simplest ('textbook') model which typically gives errors of the order of 20%, each of the other approximate models generally provides good estimates of the overall heat transfer coefficient and the rate of transfer through the exposed tube surface. Model 2 is recommended for engineering purposes where quick, relatively accurate, overall estimates are needed without recourse to a computer. This model employs one-dimensional electrical resistance analogues for both the fin and the tube, with radial conduction occurring separately in the exposed and finned tube sections and tangential conduction in the insulated portion. Model 4 is recommended as an accurate approximate model for cases where finite difference solutions are not practical, but a computer is available. This is the only model which yields consistently good estimates of the fin contribution to the overall heat transfer. It also provides excellent nodal temperature values to initiate the iterative finite difference solution (Model 5).

(4) The connecting fins generally enhance heat transfer from the hot fluidized bed to the coolant inside the tubes by increasing the furnace-side surface area and by directing the heat into the insulated sector of the tubes. Augmentation of the overall heat transfer improves with increasing tube and fin thickness, increasing fin width, increasing fin thermal conductivity and increasing thermal resistance in the fin–tube assembly relative to the inside and outside resistances.

Acknowledgements—The authors are grateful to the National Sciences and Engineering Research Council of Canada and to Energy, Mines and Resources Canada for financial assistance.

REFERENCES

1. R. Dolezal, *Large Boiler Furnaces*. Elsevier, Amsterdam (1967).
2. T. M. Grace, Chemical recovery from concentrated liquor. In *Chemical Recovery in the Alkaline Pulping Processes* (Edited by G. Hough), Chap. 4. Tappi Press, Atlanta (1985).
3. J. Highley and W. G. Kaye, Fluidized bed industrial boilers and furnaces. In *Fluidized Beds: Combustion and Applications* (Edited by J. R. Howard), Chap. 3. Applied Science, London (1983).
4. E. J. Oakes and F. Engstrom, Fluidized bed combustion provides for multifuel, economic cogeneration systems, *Pwr Engng* 56–59 (1982).
5. L. R. Glicksman, Heat transfer in fluidized bed combustors. In *Fluidized Bed Boilers: Design and Application* (Edited by P. Basu), pp. 63–100. Pergamon Press, Toronto (1984).
6. J. R. Grace, Heat transfer in circulating fluidized beds. In *Circulating Fluidized Bed Technology* (Edited by P. Basu), pp. 63–80. Pergamon Press, Toronto (1986).
7. R. L. Wu, Heat transfer in circulating fluidized beds, Ph.D. Thesis, University of British Columbia, Vancouver (1989).
8. A. M. Kopeliovich and A. S. Chernov, Investigations and improvement of temperature control of diaphragm heating surfaces of gas-tight boilers, *Energomashinostroenie* No. 11, 22–27 (1982).
9. D. R. Raymond and J. W. Rauscher, Heat transfer determination in boiler waterwall tubes using fin temperature measurements, *Tappi Journal* **67**(7), 76–79 (1984).
10. F. Kreith, *Principles of Heat Transfer*, 3rd Edn. Intext Educational, New York (1973).
11. L. C. Thomas, *Fundamentals of Heat Transfer*. Prentice-Hall, Englewood Cliffs, New Jersey (1980).
12. E. M. Sparrow and L. Lee, Effects of fin base-temperature depression in a multi-fin array, *Trans. ASME, J. Heat Transfer* **97**, 463–465 (1975).
13. G. Ryskin and L. G. Leal, Orthogonal mapping, *J. Comp. Phys.* **26**, 197–217 (1978).
14. S. V. Patankar, *Numerical Heat Transfer and Fluid Flow*. Hemisphere, New York (1980).
15. F. Wenderoth, Babcock and Wilcox, Barberton, Ohio, Personal communication, May (1986).

TRANSFERT THERMIQUE DANS DES MEMBRANES A CHUTE D'EAU

Résumé—La conduction thermique dans des assemblages de membrane à chute d'eau consistant en des tubes connectés par des ailettes longitudinales est analysée pour des conditions typiques de bouilleurs à lit fluidisés. Quatre modèles analytiques approchés sont traités avec un modèle exact numérique qui emploie une méthode aux différences finies et une transformation de coordonnées orthogonales. Les modèles approchés ont une précision d'autant meilleure que leur degré de sophistication augmente. On considère un domaine de conditions pour montrer l'influence sur le coefficient de transfert global des facteurs comme l'épaisseur du tube, l'épaisseur et la largeur de l'ailette, les coefficients de transfert thermique interne et externe, les conductivités thermiques du tube et de la paroi. On montre que l'efficacité de l'ailette et celle du secteur isolé du tube sont étroitement liées.

WÄRMEÜBERGANG IN KESSEL-FLOSSENWÄNDEN

Zusammenfassung—Flossenwände von Dampfkesseln bestehen aus Rohren, die mit Längsrippen untereinander verbunden sind. Die Wärmeleitung in derartigen Flossenwänden wird für die typischen Bedingungen von Wirbelschichtfeuerungen analytisch untersucht. Es werden vier analytische Näherungsmodelle entwickelt, außerdem ein exaktes numerisches Modell, welches auf einem Finite-Differenzen-Verfahren und einer Transformation körperangepaßter orthogonaler Koordinaten aufbaut. Ganz allgemein sind die Näherungsmodelle umso besser, je aufwendiger sie gebaut sind. Es wird eine Reihe von Fällen betrachtet, um den Einfluß folgender Größen auf den Wärmedurchgangskoeffizienten zu zeigen: Dicke der Rohre, Dicke und Breite der Rippen, innerer und äußerer Wärmeübergangskoeffizient und die Wärmeleitfähigkeiten des Rohr- und des Wandmaterials. Es zeigt sich, daß die Wirkungsgrade der Rippe und des isolierten Sektors der Rohre eng zusammenhängen.

ТЕПЛОПЕРЕНОС В МЕМБРАННЫХ ВОДООХЛАЖДАЕМЫХ ЭКРАНАХ

Аннотация—Анализируется кондуктивный теплопереноса в трубах, соединенных продольными ребрами и образующих мембранный водоохлаждаемый экран, часто применяемый в котлах с кипящим слоем. Наряду с четырьмя приближенными аналитическими моделями разработана точная численная модель, использующая конечно-разностный метод и ортогональное преобразование координат, отсчитываемых от границы. Точность приближенных моделей, как правило, возрастает при увеличении степени их сплошности. Исследуется ряд условий для иллюстрации влияния таких факторов, как толщина трубы, толщина и ширина ребра, коэффициенты внутреннаго и внешнего теплопереноса, а также теплопроводность стенки трубы и ребра на суммарный коэффициент теплопереноса. Показано, что между Эффективностью ребра и изолированного участка трубы существует тесная взаимосвязь.